NANO LETTERS

Letter

pubs.acs.org/NanoLett

Doubling Absorption in Nanowire Solar Cells with Dielectric Shell Optical Antennas

Sun-Kyung Kim,[†] Xing Zhang,[‡] David J. Hill,[‡] Kyung-Deok Song,[§] Jin-Sung Park,[§] Hong-Gyu Park,*[,§] and James F. Cahoon*[,‡]

[†]Department of Applied Physics, Kyung Hee University, Gyeonggi-do 446-701, Republic of Korea

[‡]Department of Chemistry, University of North Carolina at Chapel Hill, Chapel Hill, North Carolina 27599-3290, United States

[§]Department of Physics, Korea University, Seoul 136-701, Republic of Korea

Supporting Information

ABSTRACT: Semiconductor nanowires (NWs) often exhibit efficient, broadband light absorption despite their relatively small size. This characteristic originates from the subwavelength dimensions and high refractive indices of the NWs, which cause a light-trapping optical antenna effect. As a result, NWs could enable high-efficiency but low-cost solar cells using small volumes of expensive semiconductor material. Nevertheless, the extent to which the antenna effect can be leveraged in devices will largely determine the economic viability of NW-based solar cells. Here, we demonstrate a simple, low-cost, and scalable route to dramatically enhance the optical antenna effect in NW photovoltaic devices by coating the wires with conformal dielectric shells. Scattering and absorption measurements on Si NWs coated with shells of SiN_x or SiO_x exhibit a broadband enhancement of light absorption by ~50−200% and light scattering by ~200−1000%. The increased light−matter interaction leads to a ~80% increase in short-circuit current density in Si photovoltaic devices under 1 sun illumination. Optical simulations reproduce the experimental results and indicate the dielectric−shell effect to be a general phenomenon for groups IV, II−VI, and III−V semiconductor NWs in both lateral and vertical orientations, providing a simple route to approximately double the efficiency of NW-based solar cells.

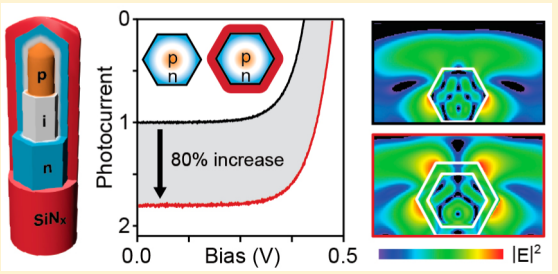

KEYWORDS: *Solar energy, photovoltaic device, silicon nanowires, optical antenna, FDTD simulation*

Semiconductor nanowires (NWs) have been widely developed for photonic and optoelectronic applications ranging from ultrasmall light sources and highly sensitive optical probes to efficient light-to-electric power converters.[1−13] Electronically active NWs incorporating p-type/n-type (p−n) or p-type/intrinsic/n-type (p−i−n) junctions have been synthesized in axial and radial geometries[14,15] with a range of materials, including groups IV,[6,16−19] II−VI,[20,21] and III−V[9,22,23] semiconductors. The p−i−n structures have been used as light-emitting diodes,[24] sensors,[25] photodetectors,[16] and photovoltaic (PV) devices.[3−5] For PV devices, InP NWs with axial p−i−n junctions have produced a 13.8% power-conversion efficiency (η) for an array of vertically oriented NWs.[9] Similarly, a single, vertical GaAs NW with a p−i−n core/shell structure has been shown to produce an apparent current density exceeding 180 mA/cm^2 because the scattering cross section greatly exceeds the physical cross section (i.e., an optical antenna effect).[10] In addition, Si NWs with radial p−i−n junctions exhibited a η of up to 6% in a single-wire, horizontal configuration.[6] For each of these devices, the key advantages of the NW structure are the unconventional light absorption characteristics caused by localized two-dimensional resonant modes, which give rise to a light-trapping optical antenna effect and a substantially increased short-circuit current density (J_{SC}) in devices.[6,7,11] In most cases, NWs can produce J_{SC} values several times larger than the values expected from bulk structures with similar material volumes.[6,9,10]

Optical resonator modes have been observed in the absorption and scattering spectra of Ge[11] and Si[6−8,26] NWs. The amplitude and frequency of the modes depends primarily on the size, cross-sectional geometry, and orientation of the wires. Here, we show that the addition of a conformal dielectric shell, as shown in Figure 1, dramatically enhances the light−matter interaction (e.g., light absorption and scattering), providing a facile and low-cost route to increase the J_{SC} of NW devices. Coatings of dielectric materials such as silicon nitride (SiN_x) and silicon oxide (SiO_x) have been used as antireflection (AR) coatings for conventional planar materials and can be deposited by low-cost plasma-enhanced chemical vapor deposition (PECVD) processes.[27] For a single dielectric material, an AR effect for planar material occurs over a relatively narrow wavelength range, and thus complex dielectric stacks[27] or textured surfaces[28] are required to produce broadband AR effects. In analogy to planar structures, we have used PECVD to

Received: November 20, 2014
Revised: December 11, 2014

DOI: 10.1021/nl504462e
Nano Lett. XXXX, XXX, XXX−XXX

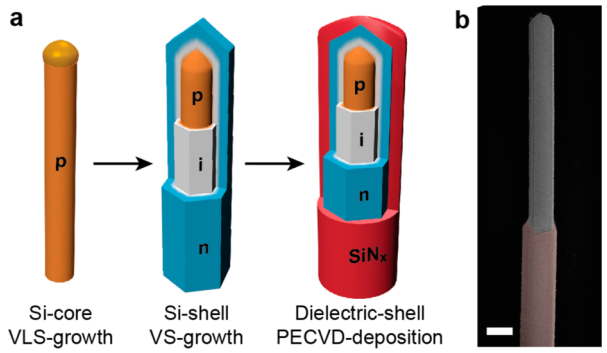

Figure 1. Fabrication of Si NWs with conformal dielectric shells. (a) Illustration of sequential VLS synthesis of p-type NWs, vapor–solid (VS) growth of intrinsic and n-type Si shells, and PECVD dielectric shell deposition. (b) False-colored SEM image of a core/shell p–i–n Si NW coated with a SiN_x dielectric shell that has been selectively removed from the upper portion of the wire to reveal the underlying Si; scale bar, 200 nm.

coat NWs with conformal dielectric shells. We experimentally measure the effect of the dielectric shell on the absorption and scattering spectra of single Si NWs, and we find that the shells produce a light–matter interaction several times larger than what would be expected from a ray-optics perspective. The results are compared to finite-difference time-domain (FDTD) simulations, which quantitatively reproduce the results. In contrast to conventional AR coatings for planar structures, dielectric shells on NWs with subwavelength diameters produce a broadband enhancement that can double light absorption in NW-based solar energy devices.

Si NWs were synthesized by the vapor–liquid–solid (VLS) mechanism in a chemical vapor deposition (CVD) reactor. For PV devices, core/shell p–i–n structures were synthesized following literature procedures[6] for VLS growth of p-type NWs followed by vapor–solid (VS) growth of intrinsic and n-type shells (Figure 1a).[29] As-grown NWs were coated with dielectric shells of SiN_x or SiO_x by PECVD on the growth substrate, as shown schematically in Figure 1a and by the scanning electron microscopy (SEM) image in Figure 1b. Single-NW PV devices were fabricated following procedures reported previously,[6] and all optical characterization was performed with NWs lying horizontally on substrates after mechanical transfer from the growth wafers.[30]

To probe the effect of the dielectric shell on the light scattering characteristics of the Si NWs, the shell was selectively removed from one-half of single wires to directly compare the scattering signal[31] from regions with and without it. As shown in Figure 2a, the dielectric shell dramatically increases the light scattered from the wire, causing higher contrast in the dark-field image. Measured scattering spectra (Figure 2b) show an increase in the scattering amplitude uniformly across the entire visible and near-infrared spectrum, and thicker shells produce substantially more scattering. Integrated over all measured wavelengths, the scattering signal from NWs coated with a ~25 nm SiN_x shell increases by ~120% but with a ~125 nm shell increases by ~800%. FDTD simulations[32] that account for the geometry of the dark-field experiment[31] reproduce the measured spectra (see dashed lines in Figure 2b). In addition, scattering field profiles were acquired at peak wavelengths in the spectra (Figure 2c). The scattering field profiles labeled 1 and 2 in the uncoated NW are dramatically enhanced by the dielectric shell, as shown by the corresponding modes labeled 4 and 5 for the coated NW. A third peak (labeled 3 for the uncoated wire and 6 for the coated wire) is primarily concentrated in the dielectric shell and also leads to enhanced scattering. The peaks labeled 1 and 2 are assigned to degenerate TEM_{11} Mie scattering resonant modes (Supporting Information, Figure S1), which verifies the direct connection between the optical antenna effect and localized resonant modes.

Scattering spectra were also measured from a core/shell p–i–n NW ~250 nm in diameter and coated with a SiN_x dielectric shell of ~50 nm. In comparison to the spectrum for the 100 nm Si NW with a ~125 nm SiN_x shell (blue solid curve in Figure 2b), the scattering spectrum for the 250 nm Si NW with a ~50 nm SiN_x shell (blue solid curve in Figure 2d) is more complex, showing multiple peaks that are enhanced in amplitude by ~250% on average. Because of the large diameter

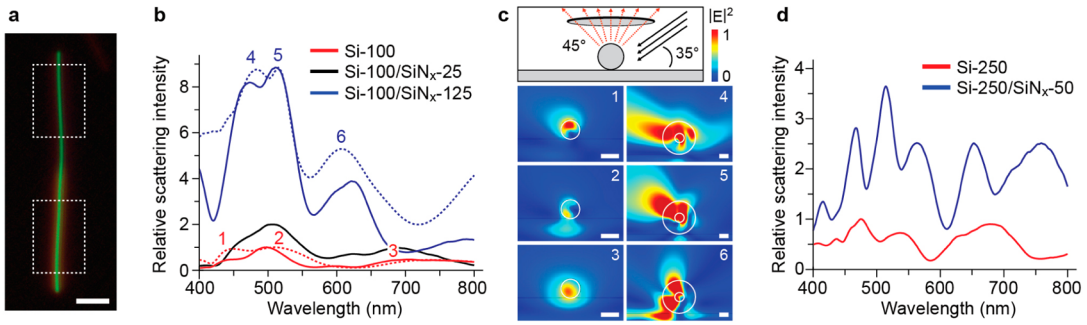

Figure 2. Light scattering from Si NWs with SiN_x dielectric shells. (a) Representative dark-field microscopy image of a ~100 nm Si NW with a ~65 nm SiN_x shell, which has been removed from the upper half of the wire by selective wet-chemical etching; scale bar, 5 μm. For all NWs, scattering spectra were collected from regions with and without the dielectric shell, as exemplified by the white dashed boxes. (b) Experimental scattering spectra (solid curves) collected from ~100 nm Si NWs without shell (red) and with ~25 nm (black) and ~125 nm (blue) SiN_x shells. Spectra were normalized to the maximum peak intensity from the uncoated portion of each wire. Dashed lines represent FDTD simulations of the scattering spectra, which have been scaled to the same intensity as the experimental data. (c) FDTD simulations showing the scattered field, $|E|^2$, at the wavelengths corresponding to the peaks labeled 1–6 in panel b; all scale bars, 100 nm. As illustrated by the upper schematic, the simulation includes illumination by a plane wave (black arrows) incident at 55° with respect to the substrate normal, causing light to be scattered (red dashed arrows) by the NW and collected within a cone angle of 45° with respect to the substrate normal, which accounts for the geometry of the dark-field experiment. (d) Experimental scattering spectra from ~250 nm core/shell p-i-n Si NWs without shell (red curve) and coated with a ~50 nm SiN_x shell (blue curve). The spectrum from the coated portion of the NW was normalized to the maximum peak intensity of the uncoated portion.

DOI: 10.1021/nl504462e
Nano Lett. XXXX, XXX, XXX–XXX

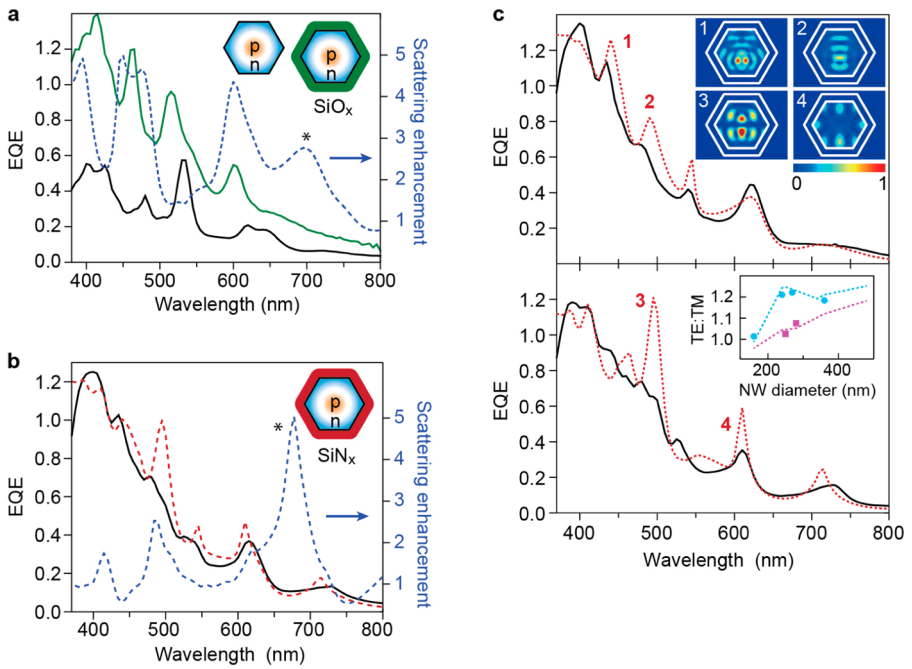

Figure 3. EQE spectra of Si core/shell p−i−n devices with SiO_x or SiN_x dielectric shells. (a) Left-hand axis: EQE experimental spectra from a 250 nm Si NW without a dielectric shell (solid black) and with a 180 nm thick SiO_x shell (solid green). Right-hand axis: simulated scattering efficiency enhancement (dashed blue) from the SiO_x shell. Insets: schematics of the p−i−n structures with and without a dielectric shell. (b) Left-hand axis: EQE experimental spectra (solid black) and simulated spectra (dashed red) for a 250 nm Si NW with ∼50 nm SiN_x shell. Right-hand axis: simulated scattering efficiency enhancement (dashed blue) from the SiN_x shell. Inset: schematic of the p−i−n structure with the dielectric shell. (c) Experimental (solid black) and simulated (dashed red) EQE spectra collected with TE (top) and TM (bottom) polarizations for a 250 nm Si NW with a 50 nm thick SiN_x shell. Upper inset: absorption mode profiles corresponding to the peaks labeled 1−4. Lower inset: simulated (dashed lines) and experimental (symbols) ratios of J_{SC} from TE and TM polarizations as a function of NW diameter for a bare Si NW (cyan dashed line and circles) and a Si NW with a 50 nm thick SiN_x shell (magenta dashed line and squares).

of the Si NW but relatively thin dielectric shell, the effect of the shell is less pronounced; however, it still more than triples the scattering amplitude for the NW. Notably, the spectral density (i.e., the number of peaks in the spectrum) of a NW cavity is retained before and after the introduction of a dielectric shell, so the NW retains the same two-dimensional localized resonant modes.

Because optical resonances serve to enhance the light−matter interaction of the NW cavity, we expect the dielectric-shell optical antenna effect to increase not only light scattering but also light absorption in PV devices.[26] In a conventional planar structure, increased reflection or backscattering from the material's front surface decreases light absorption. However, in the case of a subwavelength NW, the increase in scattering is indicative of an enhanced optical antenna effect, which increases both scattering and absorption in the NW. We examined the effect of the dielectric shell on absorption by measuring the wavelength-dependent photoresponse[33] of core/shell p−i−n PV devices with a Si diameter of ∼250 nm (Supporting Information, Figure S2). Measured external quantum efficiency (EQE) spectra are plotted in Figure 3, and spectra both without a dielectric shell and with a ∼180 nm thick SiO_x shell are shown as the black and green curves in Figure 3a, respectively. To facilitate a direct comparison of absorption with and without a dielectric shell, all spectra are calculated using the projected area of the Si portion of the NWs.[12] The spectra reveal several key features of the dielectric shell effect. First, the spectra are structured with high-contrast absorption peaks, and the spectral density and wavelengths of the peaks are approximately unchanged after introduction of the dielectric shell, as previously discussed for Figure 2d. Second, for each absorption peak, the EQE value is enhanced by a factor of ∼1.5−3.0 compared to an uncoated Si NW for all considered wavelengths. Third, the peaks between 400 and 500 nm have EQE values larger than unity and a maximum EQE value of ∼1.4 at 420 nm. We also fabricated the same p−i−n PV devices but with SiN_x shells. EQE spectra (Figure 3b) show the same broadband light absorption as SiO_x devices; however, the higher refractive index of SiN_x (∼2 compared to ∼1.5 for SiO_x) enables the same effect to be observed with a shell more than three times thinner. The measured EQE spectrum is in good agreement with the simulated absorption efficiency spectrum (red dashed curve in Figure 3b).

We calculated scattering cross sections for the SiO_x and SiN_x coated NWs, and the scattering efficiency enhancements (i.e., the ratio of the scattering cross sections from coated and uncoated NWs) are plotted as the dashed blue lines in Figure 3a and b. At each absorption peak, the scattering efficiency is significantly enhanced, which confirms that the same optical antenna effect giving rise to the enhanced scattering (Figure 2b and d) also gives rise to enhanced absorption. However, at longer wavelengths, scattering tends to be enhanced (see peaks denoted with *) without a corresponding increase in absorption. Similar to the long-wavelength peak in Figure 2b, these peaks are focused in the dielectric shell rather than Si core, reducing the absorption enhancement. Nevertheless, the broadband increase in absorption from the dielectric shell is apparent when compared to a bulk, planar structure with the same dielectric coating (Supporting Information, Figure S3),

DOI: 10.1021/nl504462e
Nano Lett. XXXX, XXX, XXX−XXX

which enhances absorption over only a narrow wavelength range.

The effect of the dielectric shell on polarization-dependent light absorption was examined with EQE spectra measured for transverse-electric (TE) and transverse-magnetic (TM) illumination. As shown in Figure 3c, each measured absorption peak is well-reproduced in the simulated spectra and can be identified as distinct two-dimensional localized modes (select modes are labeled 1−4 and depicted in the upper inset). In addition, the amplitudes of the TE and TM absorption peaks are nearly identical; in comparison, the TE absorption peaks from an uncoated NW with an equivalent Si diameter have higher amplitudes than the TM absorption peaks, particularly in the range of 400−500 nm.[7] Using simulated and experimental EQE spectra in conjunction with the AM1.5G solar spectrum, the J_{SC} polarization ratios were calculated for NWs of varying size with and without a SiN_x shell (lower inset in Figure 3c), showing good agreement between experiment and simulation. In particular, the J_{SC} polarization ratio of the NW with a SiN_x shell is close to unity if compared to an uncoated NW with a diameter greater than 150 nm, which is the smallest diameter wire with a radial p−i−n junction that has been successfully fabricated into a PV device.[7] The dielectric shell mitigates the polarization anisotropy of the NW structure and thus yields balanced light absorption between TE and TM polarizations, causing the wires to function as polarization-insensitive photon absorbers.

To evaluate the advantage of the dielectric shell for the PV characteristics of NW devices, we measured current density−voltage (J−V) transport characteristics, as shown in Figure 4a, under 1 sun AM1.5G illumination for the devices with and without a SiN_x dielectric shell ∼50 nm thick.[33] To facilitate a direct comparison, the Si projected area was used for calculation of the current density in both devices.[12] The dielectric-shell device yielded an open-circuit voltage (V_{OC}) of 0.473 V, a J_{SC} of 8.61 mA/cm^2, and a fill factor of 70%. In comparison, the device without the dielectric shell yielded a V_{OC} of 0.405 V, J_{SC} of 4.79 mA/cm^2, and a fill factor of 69%. The SiN_x thus provided both an enhancement of the voltage, most likely a result of improved surface passivation,[15] and an enhancement of the J_{SC} by ∼80%. The J_{SC} enhancement of SiN_x devices was simulated as a function of the thickness of the SiN_x shell (Figure 4b). The simulated enhancements are in good agreement with the experiment and increase monotonically for thicknesses up to ∼60 nm. The increase in J_{SC} directly results from broadband enhancement of the light−matter interaction between the incident plane wave and the optical resonator modes. This effect is apparent from a comparison of the electric field intensity ($|E|^2$) for Si wires with and without the dielectric shell (inset of Figure 4b), which shows a dramatic increase in intensity within the NW cavity after addition of the shell. However, the J_{SC} enhancement plateaus for SiN_x thicknesses greater than ∼60 nm. For thicker shells, the electric field tends to be localized in the dielectric shell region, suppressing absorption in the Si portion of the wire even though the scattering cross section continues to increase (Figure 2b).

The 1 sun photocurrent enhancement from conformal SiN_x shells is not limited to Si but rather a generic effect for group IV, II−VI, and III−V semiconductor NWs that are subwavelength in diameter. As shown by the data in Figure 4b, a SiN_x shell can be used to approximately double absorption and photocurrent not only in Si but also in CdS, GaAs, and InP

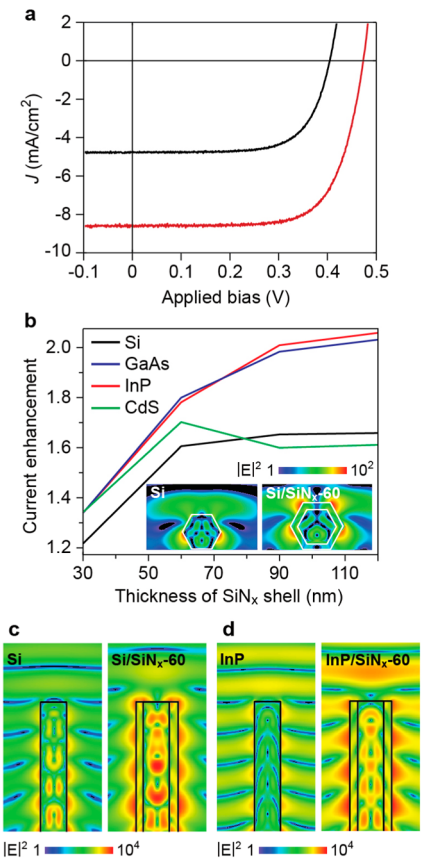

Figure 4. PV characteristics of dielectric-shell NWs under 1 sun illumination. (a) Current density−voltage characteristics under 1 sun, AM1.5G solar simulator illumination for a p−i−n ∼250 nm Si NW without a dielectric shell (solid black) and with a ∼50 nm SiN_x shell using the Si projected area to calculate the current density (solid red). (b) Simulated photocurrent enhancement as a function of SiN_x dielectric shell thickness for single, horizontally oriented NWs of Si (black), GaAs (blue), InP (red), and CdS (green). Simulations assume the AM1.5G solar spectrum and a hexagonal NW geometry with a facet-to-facet distance of 250 nm. Inset: simulations showing $|E|^2$ for a single resonant mode in a Si NW without (left) and with (right) a 60 nm thick dielectric shell. (c, d) Optical simulations showing $|E|^2$ for single, vertically oriented, 200 nm NWs without (left) and with (right) a 60 nm thick SiN_x shell for Si (panel c) and InP (panel d) materials. The length of each NW is 1 μm.

semiconductor NW materials. The exact enhancements for each material depend on the details for their optical constants and bandgaps; however, the same overall trend is apparent with all four representative semiconductor materials. In addition, the effect is present for NWs oriented vertically as well as for NWs oriented horizontally (see analogous data to Figure 4b in Supporting Information, Figure S4). As shown in Figure 4c and d, vertically oriented NWs of Si and InP, respectively, both show a dramatic amplification of the electric field intensity as a result of the dielectric shell, which is similar to the effect observed for horizontal NWs (inset of Figure 4b). Consequently, the absorption as well as scattering efficiency of wires in both lateral and vertical orientations gradually increases for SiN_x shell thicknesses up to ∼60 nm (Supporting Information, Figure S5). This dielectric-shell effect can also be leveraged in photonic applications other than PV devices, such as color-sensitive NW photodetectors that require amplification of light absorption at specific wavelengths.[7,26]

DOI: 10.1021/nl504462e
Nano Lett. XXXX, XXX, XXX−XXX

In conclusion, we have demonstrated that simple dielectric shells can double light absorption and dramatically increase light scattering in Si NWs by enhancing the optical antenna effect of the wires. The effect can be leveraged in NW-based PV devices to increase the power conversion at minimal cost by using a simple and scalable PECVD process to coat the wires. In addition, the dielectric-shell effect is generalizable to groups IV, II–VI, and III–V NWs and is present for both horizontal and vertical configurations of the wires. These results thus represent a promising step toward development of low-cost and efficient NW-based solar cells.

■ ASSOCIATED CONTENT

Supporting Information

Additional figures of optical resonances of semiconductor NWs with dielectric shells in both lateral and vertical orientations. This material is available free of charge via the Internet at http://pubs.acs.org.

■ AUTHOR INFORMATION

Corresponding Authors

*E-mail: hgpark@korea.ac.kr (H.-G.P.).
*E-mail: jfcahoon@unc.edu (J.F.C.).

Notes

The authors declare no competing financial interest.

■ ACKNOWLEDGMENTS

We thank Prof. Charles M. Lieber for providing a portion of the experimental setup. We thank R. W. Day for helpful discussions. S.-K.K. acknowledges support of this work by Basic Science Research Program through the National Research Foundation of Korea (NRF) funded by the Ministry of Science, ICT & Future Planning (NRF-2013R1A1A1059423). H.-G.P. acknowledges support of this work by the National Research Foundation of Korea (NRF) grant funded by the Korean government (MSIP) (No. 2009-0081565). D.J.H, X.Z., and J.F.C. acknowledge support by start-up funding from UNC-Chapel Hill and equipment supported by the National Science Foundation (DMR-1308695).

■ REFERENCES

(1) Lieber, C. M. *MRS Bull.* **2011**, *36*, 1052–1063.
(2) Dasgupta, N. P.; Sun, J.; Liu, C.; Brittman, S.; Andrews, S. C.; Lim, J.; Gao, H.; Yan, R.; Yang, P. *Adv. Mater.* **2014**, *26*, 2137–2184.
(3) Kempa, T. J.; Day, R. W.; Kim, S.-K.; Park, H.-G.; Lieber, C. M. *Energy Environ. Sci.* **2013**, *6*, 719–733.
(4) Garnett, E. C.; Brongersma, M. L.; Cui, Y.; McGehee, M. D. *Annu. Rev. Mater. Res.* **2011**, *41*, 269–295.
(5) Hochbaum, A. I.; Yang, P. D. *Chem. Rev.* **2010**, *110*, 527–546.
(6) Kempa, T. J.; Cahoon, J. F.; Kim, S.-K.; Day, R. W.; Bell, D. C.; Park, H.-G.; Lieber, C. M. *Proc. Natl. Acad. Sci. U.S.A.* **2012**, *109*, 1407–1412.
(7) Kim, S.-K.; Day, R. W.; Cahoon, J. F.; Kempa, T. J.; Song, K.-D.; Park, H.-G.; Lieber, C. M. *Nano Lett.* **2012**, *12*, 4971–4976.
(8) Cao, L.; Fan, P.; Vasudev, A. P.; White, J. S.; Yu, Z.; Cai, W.; Schuller, J. A.; Fan, S.; Brongersma, M. L. *Nano Lett.* **2010**, *10*, 439–445.
(9) Wallentin, J.; Anttu, N.; Asoli, D.; Huffman, M.; Aberg, I.; Magnusson, M. H.; Siefer, G.; Fuss-Kaliuweit, P.; Dimroth, F.; Witzigmann, B.; Xu, H. Q.; Samuelson, L.; Deppert, K.; Borgstrom, M. T. *Science* **2013**, *339*, 1057–1060.
(10) Krogstrup, P.; Jorgensen, H. I.; Heiss, M.; Demichel, O.; Holm, J. V.; Aagesen, M.; Nygard, J.; Fontcuberta i Morral, A. *Nat. Photonics* **2013**, *7*, 306–310.
(11) Cao, L.; White, J. S.; Park, J.-S.; Schuller, J. A.; Clemens, B.-M.; Brongersma, M. L. *Nat. Mater.* **2009**, *8*, 643–647.
(12) Yu, Y.; Ferry, V. E.; Alivisatos, A. P.; Cao, L. *Nano Lett.* **2012**, *12*, 3674–3681.
(13) Liu, W. F.; Oh, J. I.; Shen, W. Z. *IEEE Electron Device Lett.* **2011**, *32*, 45–47.
(14) Tian, B.; Kempa, T. J.; Lieber, C. M. *Chem. Soc. Rev.* **2009**, *38*, 16–24.
(15) Christesen, J. D.; Zhang, X.; Pinion, C. W.; Celano, T. A.; Flynn, C. J.; Cahoon, J. F. *Nano Lett.* **2012**, *12*, 6024–6029.
(16) Yang, C.; Barrelet, C. J.; Capasso, F.; Lieber, C. M. *Nano Lett.* **2006**, *6*, 2929–2934.
(17) Tian, B.; Zheng, X.; Kempa, T. J.; Fang, Y.; Yu, N.; Yu, G.; Huang, J.; Lieber, C. M. *Nature* **2007**, *449*, 885–889.
(18) Kempa, T. J.; Tian, B.; Kim, D. R.; Hu, J.; Zheng, X.; Lieber, C. M. *Nano Lett.* **2008**, *8*, 3456–3460.
(19) Mohite, A. D.; Perea, D. E.; Singh, S.; Dayeh, S. A.; Campbell, I. H.; Picraux, S. T.; Htoon, H. *Nano Lett.* **2012**, *12*, 1965–1971.
(20) Fan, Z.; Razavi, H.; Do, J.-w.; Moriwaki, A.; Ergen, O.; Chueh, Y.-L.; Leu, P. W.; Ho, J. C.; Takahashi, T.; Reichertz, L. A.; Neale, S.; Yu, K.; Wu, M.; Ager, J. W.; Javey, A. *Nat. Mater.* **2009**, *8*, 648–653.
(21) Tang, J.; Huo, Z.; Brittman, S.; Gao, H.; Yang, P. *Nat. Nanotechnol.* **2011**, *6*, 568–572.
(22) Colombo, C.; Heibeta, M.; Gratzel, M.; Fontcuberta i Morral, A. *Appl. Phys. Lett.* **2009**, *94*, 173108.
(23) Dong, Y.; Tian, B.; Kempa, T. J.; Lieber, C. M. *Nano Lett.* **2009**, *9*, 2183–2187.
(24) Qian, F.; Li, Y.; Gradecak, S.; Wang, D.; Barrelet, C. J.; Lieber, C. M. *Nano Lett.* **2004**, *4*, 1975–1979.
(25) Jiang, Z.; Qing, Q.; Xie, P.; Gao, R.; Lieber, C. M. *Nano Lett.* **2012**, *12*, 1711–1716.
(26) Cao, L.; Fan, P.; Barnard, E. S.; Brown, A. M.; Brongersma, M. L. *Nano Lett.* **2010**, *10*, 2649–2654.
(27) Nagel, H.; Aberle, A. G.; Hezel, R. *Prog. Photovoltaics* **1999**, *7*, 245–260.
(28) Campbell, P.; Green, M. A. *Sol. Energy Mater. Sol. Cells* **2001**, *65*, 369–375.
(29) Si NWs were synthesized by the VLS mechanism in a home-built CVD reactor using Au nanoparticles (BBI International) dispersed on Si/SiO_x substrates (University Wafer) as catalysts and using silane (SiH_4; Voltaix), phosphine (PH_3; Voltaix, diluted to 1000 ppm), diborane (B_2H_6; Voltaix, diluted to 100 ppm), and hydrogen (H_2, Matheson 5N semiconductor grade) gases at a total pressure of 40 Torr. For scattering studies with ∼100 nm diameter wires, intrinsic NWs were nucleated at 450 °C followed by elongation at 420 °C (2.00 standard cubic centimeter per minute (sccm) SiH_4 and 200 sccm H_2) using a two-step procedure to eliminate tapering along the wire axis. Core/shell p–i–n structures were grown following literature procedures for p-type VLS wire growth at 460 °C (1.00 sccm SiH_4, 60.0 sccm H_2, 10.00 sccm B_2H_6) followed by VS intrinsic and n-type shell growth at 760 °C and 25 Torr total pressure using 0.15 sccm SiH_4, 60.0 sccm H_2, and optionally 0.75 sccm PH_3 for n-type regions. Typical VLS growth times were 1–2 h and VS shell growth times ∼40 min. NWs were coated with either SiO_x or SiN_x using standard PECVD processes at 13.56 MHz with an Advanced Vacuum Vision 310 system. NWs were imaged by SEM using a Zeiss Ultra 55 or an FEI Helios 600 Nanolab Dual Beam system.
(30) NWs and devices for optical measurements were prepared by dispersing individual NWs onto device substrates (Si wafers coated with 100 nm SiO_x and 200 nm SiN_x; Nova Electronic Materials). SU-8 (MicroChem) etch masks were defined over portions of individual NWs using electron-beam lithography followed by wet-chemical etching of SiO_x or SiN_x shells in buffered hydrofluoric acid (Transene BHF Improved) and, optionally, etching of Si in KOH solution (18.0 g KOH in 60 mL H_2O and 20 mL isopropanol at 60 °C). SU-8 was subsequently stripped using a UV/ozone dry stripper (Samco UV-1). For PV devices, electrical contacts were patterned to the n-type and p-type regions of individual NWs using electron-beam lithography with poly(methyl methacrylate) (MicroChem Corp.) resist followed by

DOI: 10.1021/nl504462e
Nano Lett. XXXX, XXX, XXX–XXX

evaporation and lift-off of ∼3 nm Ti and 300−400 nm Pd, deposited using a thermal evaporator (Sharon Vacuum) with a base pressure below 1×10^{-7} Torr.

(31) Dark-field imaging and scattering measurements were performed on isolated NWs lying horizontally on device substrates using a Zeiss AxioImager A2M upright microscope with a halogen lamp illumination source (Zeiss HAL 100) and a 50× dark-field objective (Zeiss EC Epiplan 50×/0.7 HD WD = 1.1 M27) with a numerical aperture of 0.7. The dark-field image was cropped to isolate select regions of the NWs, and spectra were collected with a spectrometer (Princeton Instruments Acton SP2500) fiber-coupled to the microscope and equipped with a liquid-nitrogen-cooled CCD array (Princeton Instruments LN/CCD-1340/400). Scattering spectra were corrected for the intensity of the light source measured with a diffuse reflectance standard (Labsphere), but dark-field images were not corrected.

(32) The absorption and scattering spectra of NWs were calculated by our home-built FDTD software. The simulated scattering spectra approximately account for the illumination angle (∼55°) and the collection angle (±45°) of the dark-field experiment, in which near-to-far field transformation was used to integrate the scattering light within the collection angle. A total-field scattered-field method was applied to discern only the scattering field from the total field (incident + scattering) and also to ensure that a single NW experiences an infinite plane wave. For absorption spectra, a normal plane wave with TE and TM polarizations was used, and $J \cdot E$ was integrated at each grid point within a NW, where J and E are the polarization current density and electric field, respectively. The J_{SC} of a NW was calculated by considering the absorption efficiency and spectral irradiance of the AM1.5G reference spectrum within the range relevant for each material (300−1000 nm for Si, InP and GaAs, and 300−580 nm for CdS). For absorption efficiency and J_{SC}, a unity internal quantum efficiency (IQE) was assumed except for the Si NWs in Figure 3b and c, where IQE was set to be 0.8. To represent a hexagonal (circular) NW, a spatial resolution of $5/\sqrt{3}$ (5), 5, and 5 nm for x, y, and z, respectively, was used, where y lies along the NW axis and z lies along the direction of the normal plane wave. All NW simulations included a 200 nm SiN_x/100 nm SiO_x/Si substrate. To model the dispersive properties of the Si and other semiconductors (CdS, InP, and GaAs), the Drude-critical points model was incorporated into the FDTD software. The plasma and collision frequencies were obtained by fitting the measured refractive index and extinction coefficient over the considered spectrum.

(33) Photocurrent measurements were acquired from individual p−i−n NW devices with a semiconductor parameter analyzer (Agilent Technologies 4156C). Using a probe station (TTP-4, Desert Cryogenics), current−voltage measurements were performed under 1 sun illumination using a solar simulator (150W, Newport Oriel) equipped with an AM1.5G filter and adjusted to an intensity of 100 mW/cm^2. EQE spectra were acquired as described previously by wire bonding to individual devices and measuring the photocurrent under wavelength- and polarization-selective illumination. The solar simulator in conjunction with a spectrometer (SpectraPro 300i, Acton Research equipped with a 1200 groove/mm grating) and a Glan-Thompson calcite polarizer (Newport 10GT04) was used as the illumination source. The illumination power density was measured using calibrated circular apertures and a certified silicon photodetector (Newport 918D-UV). Photocurrent measurements were converted to EQE values or current density (including J_{SC}) values using the power density and the projected area of the Si portion of individual NWs as measured by high-resolution SEM images. Polarized TE and TM spectra were separately collected and averaged to produce unpolarized EQE spectra.

DOI: 10.1021/nl504462e
Nano Lett. XXXX, XXX, XXX−XXX